Acta Mech
https://doi.org/10.1007/s00707-023-03623-1

ORIGINAL PAPER

Saptarshi Kumar Lahiri · **Konstantin Volokh**

Drag reduction via polymer solute: 3D numerical simulations of pipe flow

Received: 5 February 2023 / Revised: 19 April 2023 / Accepted: 4 June 2023

Abstract The mechanism of drag reduction via polymer additives is long debated in the literature. This journal published a paper (Volokh in Acta Mech 229(10):4295–4301, 2018), in which the drag reduction was explained based on the Navier–Stokes model enhanced with the viscous strength. This explanation was limited by a qualitative consideration of the onset of material instability in the laminar pipe flow. In the present work, we use the theoretical setting of Volokh (2018) in 3D numerical simulations of the realistic pipe flow where material instabilities develop into turbulence. We observe in the simulations that the addition of the polymer solute suppresses the chaotic turbulent motion, indeed, in accordance with the experimental observations of the phenomenon.

1 Introduction

The use of polymer additives as drag-reducing agents in turbulent flows is an economical practice and finds remarkable engineering applications. Toms [2] first reported the phenomenon of drag reduction using small amounts of additives to the Newtonian solvent. Since then a vast literature is available on the topic, primarily experimental in nature. For this, we can refer to the extensive bibliographical account in [3–5]. The relevant recent reviews can be found in [6–14].

Despite such an enormous volume of experimental works, the theoretical explanation of drag reduction has been long debated, possibly because the process of the transition to turbulence is yet to be understood properly. In its first explanation, Oldroyd [15] suggested that the addition of polymer caused a flow slip near the wall that reduced the drag. However, his hypothesis was questioned by Tanner and Walters [16] as the solvent did not slip at the boundaries. In another possible explanation De Gennes [17] suggested that the storage and release of energy by the polymer molecules reduced the drag by reducing the momentum flux near the wall. This argument was contested by L'vov et al. [18] and Procaccia et al. [19] stating that the microscopic contributions of polymer energy were unlikely to change the rate of energy flux, determined by the forcing mechanism at the macroscopic scale. L'vov et al. [18] assumed that the primary cause behind the drag reduction was the reduction in momentum flux from the bulk to the wall and they proposed an effective viscosity function that increased with distance from the wall. This assumption needs further investigation.

Lumley [20] observed that the added polymers made fluid particles to move less chaotically and faster reducing the drag. Hence, it is rather important to understand the role of polymer additives in the turbulent flow of the solvent. The polymer molecules certainly help to suppress the local flow instabilities and, thus,

S. K. Lahiri (✉)· K. Volokh
Faculty of Civil and Environmental Engineering, Technion – Israel Institute of Technology, Haifa 3200003, Israel
E-mail: lahiriayan22@gmail.com

K. Volokh
E-mail: cvolokh@technion.ac.il

Published online: 18 June 2023

they can qualitatively explain the drag reduction via the delayed transition to turbulence of laminar pipe flows. Reynolds number ($\mathrm{Re} = \rho v D/\eta$; where ρ is the density, η is the viscosity, v is the velocity of flow, and D is the diameter of the cross-section of the channel) [21,22] is the controlling parameter to decide whether the pipe flow remains laminar or turbulent in nature. Although experimental observations [23–26] suggest an approximate range of $1600 < \mathrm{Re}_{\mathrm{cr}} < 3000$ for the transition to turbulence, it is well established that the standard Navier–Stokes (N–S) constitutive model ensures linear stability for the shear flow problems [27,28] and is unable to explain the transition to turbulence. While the presence of finite perturbation has been thought of as a possible reason for [24,29] generating kinematic instabilities of the flow, disturbances often decay along the flow and not always necessarily cause turbulence [30]. Hence kinematic instabilities might not be adequate for the explanation of the transition to turbulence and, perhaps, we need to account for the contribution of material instabilities of the laminar flow. The option of material instability of the laminar flow was introduced in [31,32] as a Navier–Stokes model enhanced with the viscous strength. The latter continuum mechanics setting was further confirmed by molecular dynamic simulations reported in [33].

Volokh [1] used the viscous strength model to explain the drag reduction. Analytical considerations reported in [1] are rather qualitative. In the present work, we report the results of numerical simulations of 3D pipe flows with polymer additives. The results show, indeed, that the solute can reduce the developed turbulence.

2 Navier–Stokes model with viscous strength

The classical N–S model fails to explain the transition to turbulence in the pipe flow. Volokh [31,32] assumed that material instabilities should be allowed by the constitutive model and he proposed the viscous strength model (VSM). In the latter model, the shear stresses generated within the flow possess an upper cap (termed as the '*viscous strength*') and cease to exist as the strain rate exceeds the critical value. Once the viscous limit is passed, the flow behaves as an ideal fluid with almost zero viscosity. During this transition from the standard viscous Newtonian fluid flow to the ideal fluid flow, infinitesimal perturbations grow into finite ones and initiate the transition to turbulence [31,32,34]. Remarkably, Raghavan and Ostoja-Starzewski [33] also reported similar observations on the strength of fluids in the context of molecular dynamics.

In VSM, the flow is described by the standard law of the balance of linear momentum in the form

$$\rho \frac{\partial \mathbf{v}}{\partial t} + \rho(\mathrm{grad}\mathbf{v}) \cdot \mathbf{v} = -\mathrm{grad}\, p + \mathrm{div}\boldsymbol{\tau}, \tag{1}$$

where ρ is the mass density; $\mathbf{v}$ is the velocity obeying the incompressibility condition i.e, $\mathrm{div}(\mathbf{v}) = 0$; t is time; p is the hydro-static pressure; and $\boldsymbol{\tau}$ is the viscous stress tensor.

The viscous stress is defined by the constitutive law

$$\boldsymbol{\tau} = 2\eta^* \mathbf{D}, \tag{2}$$

where $2\mathbf{D} = \mathrm{grad}\mathbf{v} + \mathrm{grad}\mathbf{v}^{\mathrm{T}}$ and η^* is the viscosity function

$$\eta^* = \eta \exp\left[-\frac{\mathbf{D} : \mathbf{D}}{\phi^2}\right]^m, \tag{3}$$

in which η is the constant viscosity of the fluid and m is a mathematical parameter dictating the sharpness of the viscosity drop beyond the critical strain rate ϕ (see Fig. 1).

Hence

$$\eta^* = \begin{cases} \eta & \text{when } \mathbf{D} : \mathbf{D} < \phi^2 \\ 0 & \text{when } \mathbf{D} : \mathbf{D} > \phi^2. \end{cases} \tag{4}$$

The viscosity function in Eq. 4 preserves the Newtonian nature of the flow. For $\mathbf{D} : \mathbf{D} < \phi^2$, the fluid behaves in accordance with the classical N–S approach, and as $\mathbf{D} : \mathbf{D} > \phi^2$, the flow exhibits ideal fluid characteristics (still Newtonian in nature with $\eta^* = 0$).

For the sake of clarification of the constitutive law, Fig. 2 shows the variation of the normalised shear stress ($\frac{\tau_{xy}}{\eta\phi}$) with normalised strain rate ($\frac{D_{xy}}{\phi}$) for a 2D flow between two parallel plates in the XY plane. The shear stress (τ_{xy}) increases with strain rate (D_{xy}) like a Newtonian fluid and attains maximum (termed as the '*viscous*

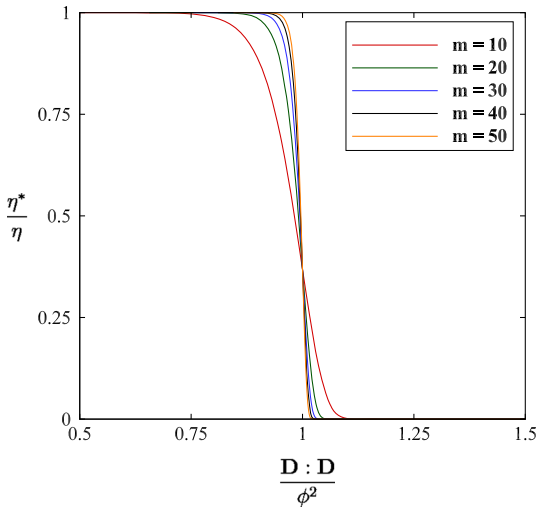

Fig. 1 Graphical representation of the variation of viscosity with strain rate

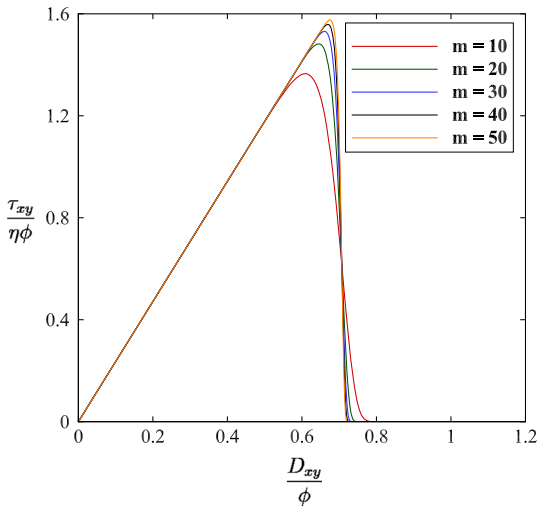

Fig. 2 Variation of shear stress with strain rate for a 2D flow between parallel plates

strength' of the fluid) before dropping to zero. We can sharpen the breakdown of friction between the fluid layers by increasing the value of m. The stress-deformation rate curve attains its maximum at

$$D_{xy} = \left[\frac{1}{2^{m+1}m}\right]^{\frac{1}{2m}}\phi, \tag{5}$$

and, hence, in the limiting case of $m \to \infty$, the viscous strength of the fluid can be analytically obtained as

$$\tau_{xy} = \sqrt{2}\eta\phi, \tag{6}$$

and, subsequently, the critical velocity becomes

$$v_{\text{cr}} = \frac{\sqrt{2}}{\sqrt[2m]{2m}}h\phi. \tag{7}$$

We note that for the perfectly intact viscosity, i.e. $\phi \to \infty$, the critical velocity approaches infinity: $v_{\text{cr}} \to \infty$; the flow becomes unconditionally stable—the case of the standard Navier–Stokes formulation. While, in the presence of the finite viscous strength, we get the limiting critical velocity: $v_{\text{cr}} = \lim_{m\to\infty}\left[\frac{\sqrt{2}}{\sqrt[2m]{2m}}h\phi\right] = \sqrt{2}h\phi$.

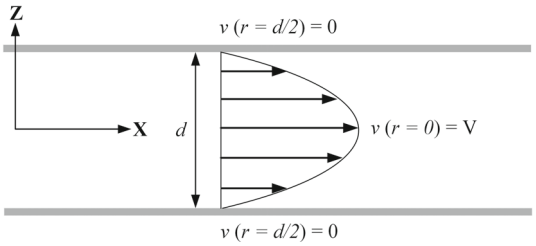

Fig. 3 Axi-symmetric flow through a pipe

3 Account of polymer additives

There are various theoretical models including the effect of polymer solutes on the flow of the solvent. For example, it is possible to add the viscous stress $\boldsymbol{\tau}^p$ due to the polymer additive in the linear momentum balance, Eq. 1, as follows

$$\rho \frac{\partial \mathbf{v}}{\partial t} + \rho \, (\text{grad}\mathbf{v}) \cdot \mathbf{v} = -\text{grad}p + \text{div}\big(\boldsymbol{\tau} + \boldsymbol{\tau}^p\big). \tag{8}$$

The constitutive relationship of the polymer stress follows the Upper Convected Maxwell model (UCM)

$$\boldsymbol{\tau}^p + \lambda \overset{\triangledown}{\boldsymbol{\tau}}^p = G\mathbf{1}, \tag{9}$$

where λ is the relaxation time; $\mathbf{1}$ is the identity tensor; and $G = n_p k_\text{B} T$ is the shear modulus [12], in which n_p is the number of molecular sub-chains per unit volume, k_B is the Boltzmann constant and T is the absolute temperature.

The Oldroyd objective rate $\overset{\triangledown}{\boldsymbol{\tau}}^p$ in Eq. 9 is defined by

$$\overset{\triangledown}{\boldsymbol{\tau}}^p = \frac{\partial \boldsymbol{\tau}^p}{\partial t} + \big(\text{grad}\boldsymbol{\tau}^p\big)\,\mathbf{v} - (\text{grad}\mathbf{v})\,\boldsymbol{\tau}^p - \boldsymbol{\tau}^p\,(\text{grad}\mathbf{v})^\cdot \tag{10}$$

Based on this formulation, Volokh [1] obtained the velocity of the laminar pipe flow (see Fig. 3)

$$v = \frac{D^2 - 4Y^2 - 4Z^2}{16\,(\eta^* + \lambda G)} \frac{\partial p}{\partial X}, \tag{11}$$

in which we have $\eta^* \to 0$ for any strain rate exceeding the critical value, i.e. $\mathbf{D} : \mathbf{D} > \phi^2$, and the flow is stabilized by the polymer additive via λG term.

4 Numerical simulations of 3D pipe flow with additives

In this section, we present results of simulations of the flow through a straight cylindrical three-dimensional pipe of 60 mm length and a uniform circular cross-section of $D = 4$ mm diameter (see Fig. 4) with the polymeric stress in addition to the viscous strength. The material flowing through the pipe is water with mass density $\rho = 1000\,\text{kg/m}^3$ and viscosity $\eta = 0.001\,\text{kg/ms}$. The values of the viscous strength parameters $m = 20$, and $\phi = 848.5\,\text{s}^{-1}$ were calibrated in [32].

We note, in passing, that the numerical simulations of the pipe flow without the polymer additives are reported in [34].

4.1 Numerical framework

The 3D flow in the pipe is discretized with 1,514,133 nodes in the commercial software ANSYS-2021R2 [35]. Figure 5 shows the mesh at a typical cross-section. The boundary of the pipe section is assumed to be perfectly smooth to avoid any additional perturbation within the system, and the inlet is provided with a parabolic velocity profile to ensure a fully developed flow regime. We adopt the large eddy simulation (LES) [36] approach, which is computationally effective and can capture the transition to turbulence with reasonable

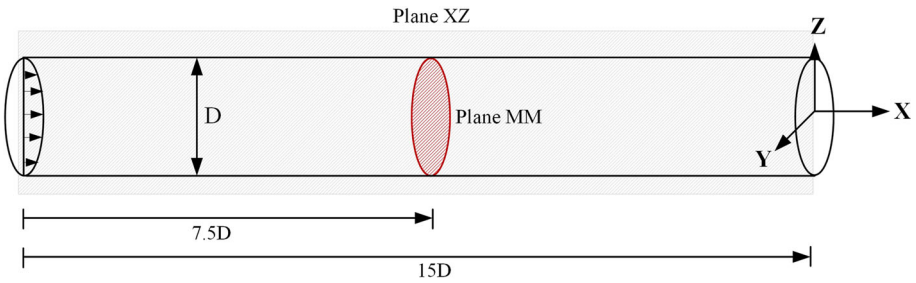

Fig. 4 Schematic diagram: flow through a straight cylindrical pipe with uniform circular cross-section

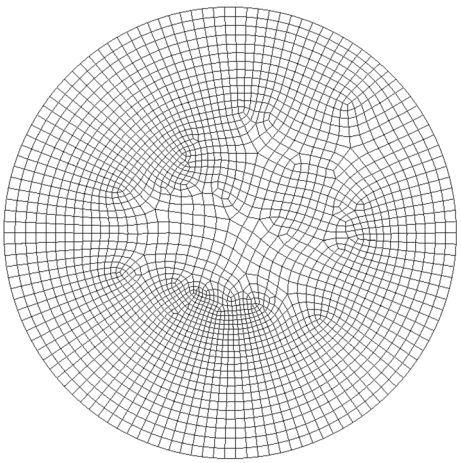

Fig. 5 Discretization at a typical cross-section of the numerical model in ANSYS2021R2

Table 1 Inlet velocity (v_{in}) and Reynolds number (Re) for numerical case studies ($\rho = 1000\,\text{kg/m}^3$; $D = 4\,\text{mm}$; $\eta = 0.001\,\text{kg m}^{-1}\,\text{s}^{-1}$)

Load case	Inlet velocity (v_{in}) (m/s)	$\text{Re} = \frac{2\rho v_{\text{in}} D}{3\eta}$
A	0.8	2133
B	0.9	2400

accuracy. Among the available sub-grid turbulence models, we incorporate the Wall Adopted Local Eddy-Viscosity (WALE) [37] approach, which is specifically advantageous for problems related to transitional flows. We consider $C_{\text{W}} = 0.325$, which has been reported to ensure satisfactory results over a wide range of Reynolds numbers [35]. The LES-WALE model of the transient pipe flow is solved within a pressure-based solver by the bounded second-order implicit numerical scheme with a stable time increment of $1.0\,\text{e}^{-5}$ s.

Table 1 lists the inlet velocities and corresponding Reynolds numbers considered in numerical examples. For a parabolic velocity profile with peak v_{in} at the inlet of the pipe, an approximate estimate of the corresponding Reynolds number (Re) can be calculated from the average velocity generated within the flow. Generally, for laminar flow, the average flow velocity is related to the peak velocity as $v_{\text{av}} = 2v_{\text{in}}/3$. We consider a relaxation time $\lambda = 0.6$ s and viscosity $\eta = 0.001\,\text{kg m}^{-1}\,\text{s}^{-1}$ for all the numerical problems in this paper.

4.2 Case study A

We consider the peak velocity $v_{\text{in}} = 0.8\,\text{m/s}$ and present a comparative study between the numerical predictions of four different models:

1. standard Navier–Stokes model without polymer;
2. viscous strength model (VSM) without polymer: $G = 0\,\text{Pa}$;

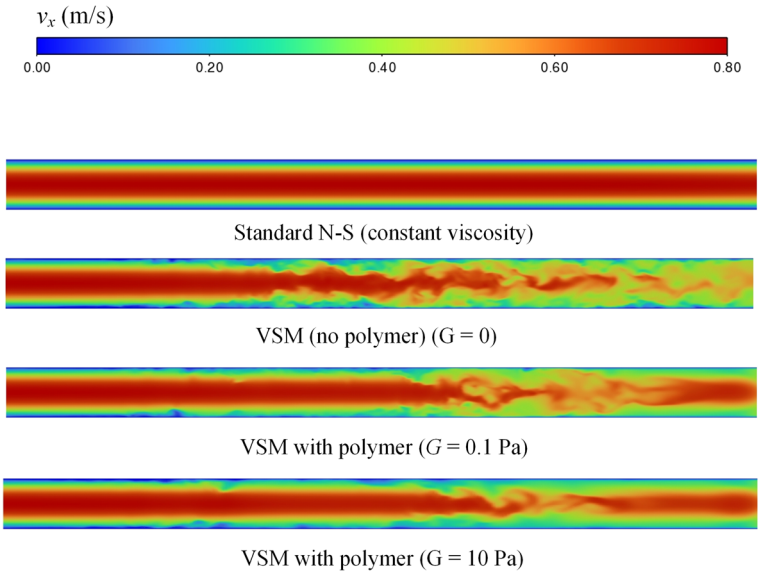

Fig. 6 Profile of longitudinal velocity (v_x) profile in plane XZ (see Fig. 4) for different polymer concentrations with $v_{\text{in}} = 0.8$ m/s

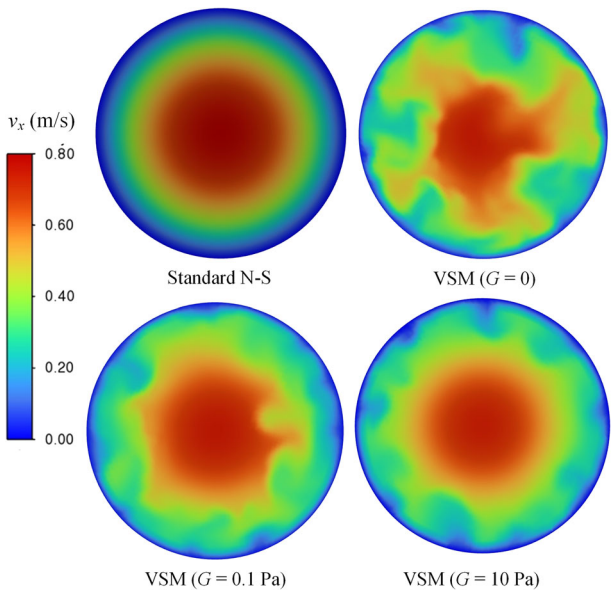

Fig. 7 Contour of longitudinal velocity (v_x) profile in plane MM (see Fig. 4) for different polymer concentrations with $v_{\text{in}} = 0.8$ m/s

3. viscous strength model with polymer: $G = 0.1$ Pa;
4. viscous strength model with polymer: $G = 10$ Pa.

Figures 6, 7, 8 and 9 present the variation of longitudinal and transverse velocity profiles in plane XZ (see Fig. 4) along the length of the pipe for all models. The longitudinal velocity profile (Fig. 6) suggests that the standard N–S approach (1) predicts a perfectly stable laminar solution, whereas the viscous strength model (2) predicts turbulence within the flow. By adding mixing polymer within the solution (i.e. considering the effect of polymer shear modulus, G)—models (3) and (4)—we observe a reduction in turbulence. We can draw a similar conclusion from the variation of transverse velocities in Figs. 8 and 9, where the transverse perturbations do not exist for the standard N–S model, and significant perturbations occur for VSM model, which reduces with the addition of polymer. Although $G = 0.1$ Pa stabilises the flow, it does not completely

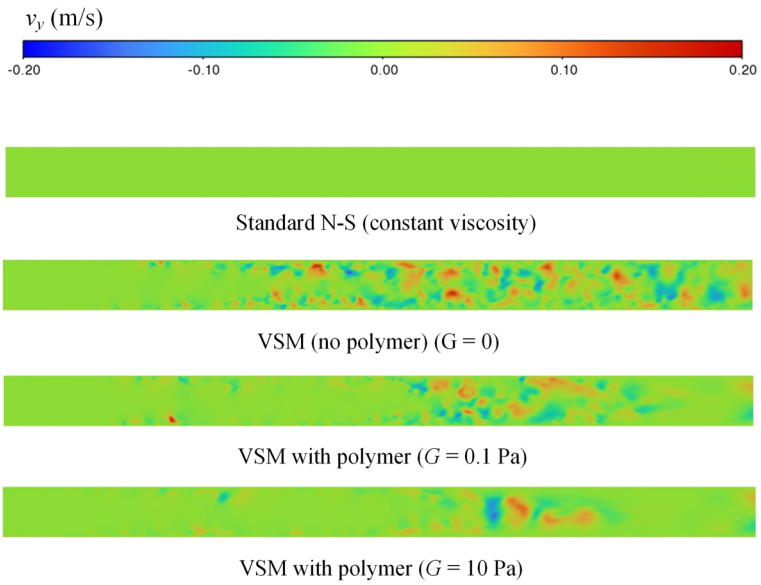

Fig. 8 Profile of transverse velocity (v_y) profile in plane XZ (see Fig. 4) for different polymer concentrations with $v_{\text{in}} = 0.8$ m/s

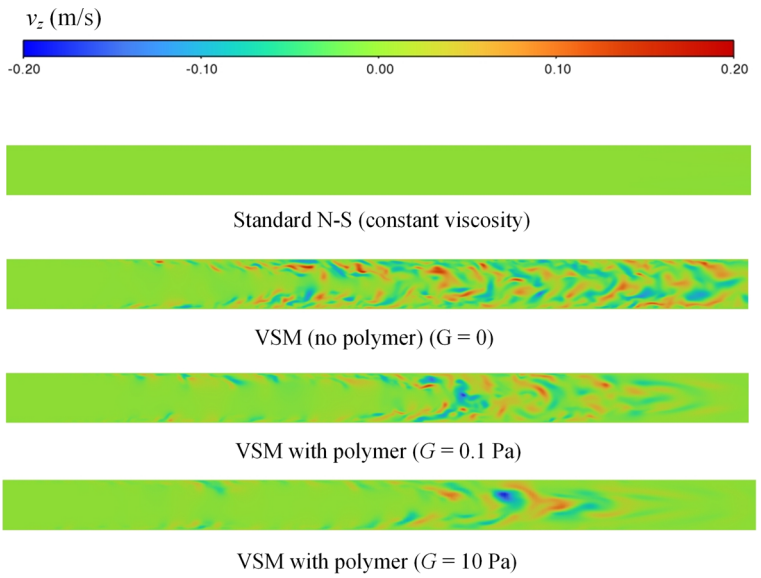

Fig. 9 Profile of transverse velocity (v_z) profile in plane XZ (see Fig. 4) for different polymer concentrations with $v_{\text{in}} = 0.8$ m/s

restore the laminar nature of the flow. To further study the contribution of G, we consider the next case study with a peak inlet velocity of 0.9 m/s.

4.3 Case study B

We increase the peak inlet velocity to 0.9 m/s with four different polymer shear moduli: $G = 0, 0.1, 1.0, 100$ Pa. We present the contour maps of velocities in longitudinal and transverse directions in Figs. 10, 11, 12 and 13 for all simulation models. Figure 10 indicates that the standard N–S model (1) predicts a perfectly laminar longitudinal flow profile, but the viscous strength model (2) exhibits a transition to turbulence in the flow. This numerical result also fits the experiments reported in [26], in which transition to turbulence was observed at $\text{Re} \approx 2400$.

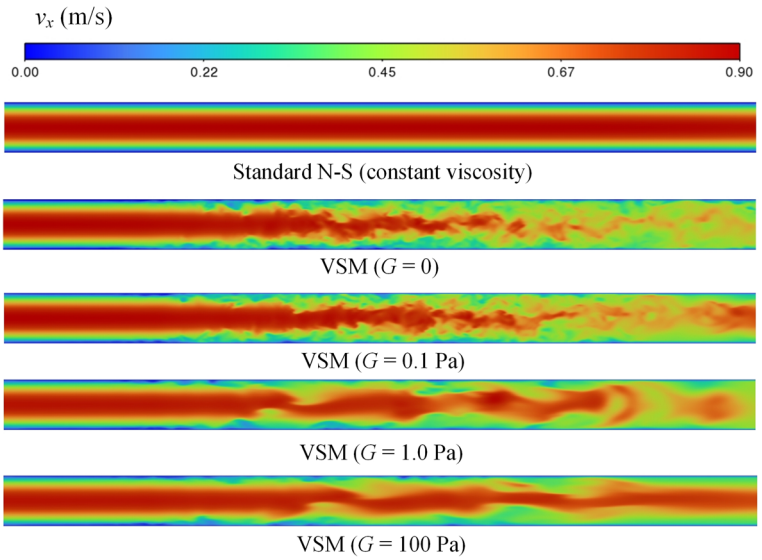

Fig. 10 Profile of longitudinal velocity (v_x) profile in plane XZ (see Fig. 4) for different polymer concentrations with $v_{\text{in}} = 0.9$ m/s

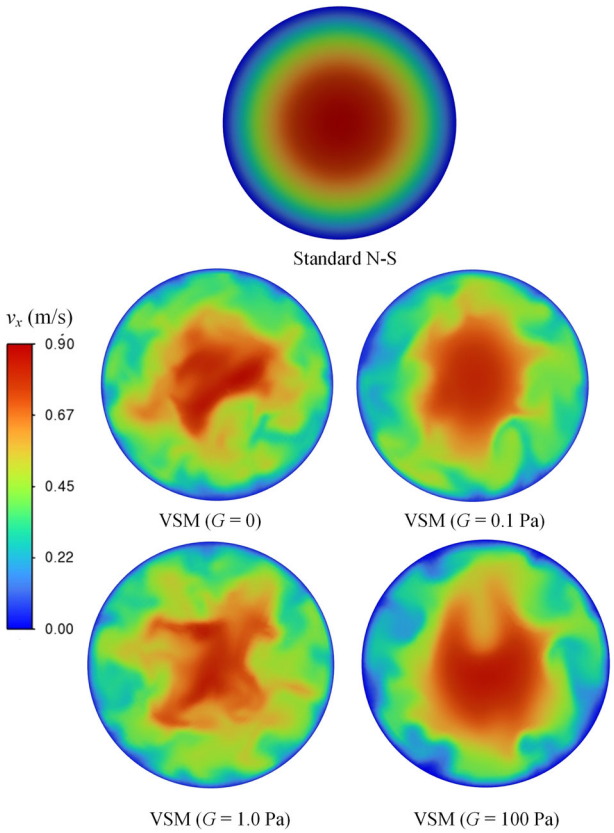

Fig. 11 Contour of longitudinal velocity (v_x) profile in plane MM (see Fig. 4) for different polymer concentrations with $v_{\text{in}} = 0.9$ m/s

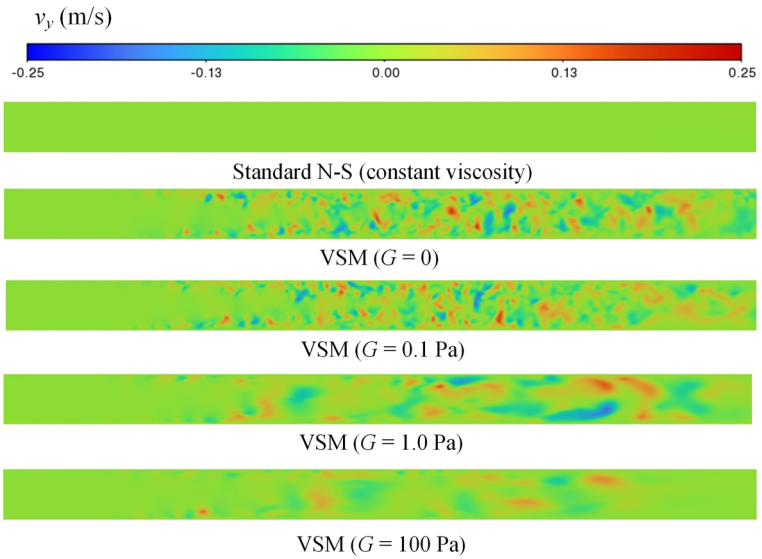

Fig. 12 Profile of transverse velocity (v_y) profile in plane XZ (see Fig. 4) for different polymer concentrations with $v_{\text{in}} = 0.9$ m/s

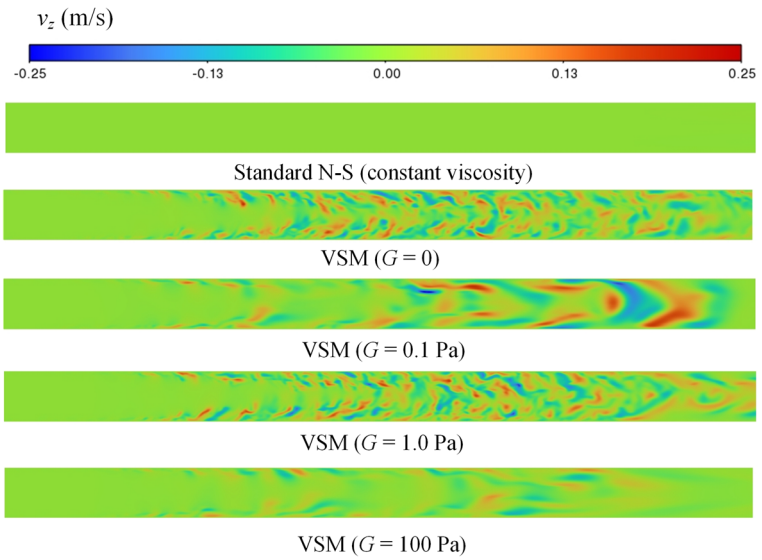

Fig. 13 Profile of transverse velocity (v_z) profile in plane XZ (see Fig. 4) for different polymer concentrations with $v_{\text{in}} = 0.9$ m/s

By adding polymer with shear modulus G, it is possible to stabilize and laminarize the turbulent flow—Fig. 10 —with a significant reduction in the transverse perturbations in the pipe—Figs. 12 and 13.

4.4 Reduction in wall shear stress

The polymer additives reduce the shear stress generated at the wall of the pipe section significantly. The maximum wall shear stress are listed in Tables 2 and 3 for two inlet velocity cases $v_{\text{in}} = 0.8$ and 0.9 m/s. We note—Fig. 14—that the transition to turbulence from laminar flow significantly increases the wall shear stress when no polymer is added to the solvent. The addition of polymer reduces the drag causing a decrease in the maximum wall shear stress. For $v_{\text{in}} = 0.8$ m/s, the contribution of polymer to shear modulus of $G = 0.1$ Pa reduces the wall shear stress by $\approx 18\%$. For $v_{\text{in}} = 0.9$ m/s, the contribution of polymer to shear modulus of $G = 100$ Pa reduces the wall shear stress by $\approx 47\%$.

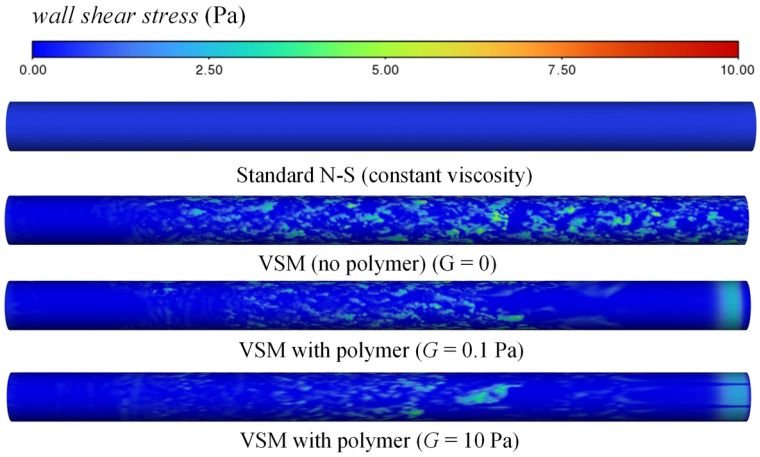

Fig. 14 Contour of shear stress (Pa) at the wall of the pipe section with increasing amount of polymer

Table 2 Maximum wall shear stress (Pa) for $v_{\text{in}} = 0.8\,\text{m/s}$

Standard N–S $G = 0\,\text{Pa}$	VSM $G = 0\,\text{Pa}$	VSM $G = 0.1\,\text{Pa}$	VSM $G = 10\,\text{Pa}$
0.8	8.8	7.20	5.11

Table 3 Maximum wall shear stress (Pa) for $v_{\text{in}} = 0.9\,\text{m/s}$

Standard N–S $G = 0\,\text{Pa}$	VSM $G = 0\,\text{Pa}$	VSM $G = 0.01\,\text{Pa}$	VSM $G = 0.1\,\text{Pa}$	VSM $G = 100\,\text{Pa}$
0.9	13.68	13.12	10.86	7.12

5 Closure

In this work we numerically simulated pipe flow of water with polymer additives. Beyond the critical Reynolds number of ≈ 2400 the laminar flow becomes turbulent. Such transition cannot be described by the standard Navier–Stokes model, which only accommodates kinematic instabilities of the flow. So, we used a modified Navier–Stokes model with the finite viscous strength (VSM). The latter model accommodates both kinematic and material instabilities of the flow and it can describe the transition to turbulence in the pipe flow observed experimentally.

We further modified the VSM model to account for the polymer solute via additional viscous stress defined by the Upper Convected Maxwell model. Introduction of the polymer molecules adds strengths to the laminar flow and suppresses chaotic turbulent fluctuations. These results are the first explanation of the drag reduction via polymer solute based on the direct 3D numerical simulations. A detailed investigation of the correlation between the polymer shear modulus and the concentration of the solute would provide better physical insight into the problem and it is kept for further work.

Acknowledgements This work was supported by the Israel Science Foundation (ISF-394/20).

References

1. Volokh, K.: An explanation of the drag reduction via polymer solute. Acta Mech. **229**(10), 4295–4301 (2018)
2. Toms, B.A.: Some observations on the flow of linear polymer solutions through straight tubes at large Reynolds numbers. In: Proceedings of the First International Congress on Rheology, vol. 2, pp. 135–141 (1949)
3. Nadolink, R.H., Haigh, W.W.: Bibliography on skin friction reduction with polymers and other boundary-layer additives. Appl. Mech. Rev. **47**, 351–460 (1995)
4. Bewersdorff, H.-W.: Drag Reduction of Turbulent Flows by Additives. Kluwer, Philadelphia (1995)

5. Utomo, A., Riadi, A.: Drag reduction using additives in smooth circular pipes based on experimental approach. Processes **9**(9), 1596 (2021)
6. Gyr, A., Bewersdorff, H.-W.: Drag Reduction of Turbulent Flows by Additives, vol. 32. Springer, Berlin (2013)
7. Cadot, O., Bonn, D., Douady, S.: Turbulent drag reduction in a closed flow system: boundary layer versus bulk effects. Phys. Fluids **10**(2), 426–436 (1998)
8. Dubief, Y., et al.: On the coherent drag-reducing and turbulence-enhancing behaviour of polymers in wall flows. J. Fluid Mech. **514**, 271–280 (2004)
9. Gupta, V., Sureshkumar, R., Khomami, B.: Polymer chain dynamics in Newtonian and viscoelastic turbulent channel flows. Phys. Fluids **16**(5), 1546–1566 (2004)
10. Liberzon, A., Guala, M., Lüthi, B., Kinzelbach, W., Tsinober, A.: Turbulence in dilute polymer solutions. Phys. Fluids **17**(3), 031707 (2005)
11. Ptasinski, P., et al.: Turbulent channel flow near maximum drag reduction: simulations, experiments and mechanisms. J. Fluid Mech. **490**, 251–291 (2003)
12. Leonov, A.I., Prokunin, A.: Nonlinear Phenomena in Flows of Viscoelastic Polymer Fluids. Springer, Berlin (2012)
13. Boelens, A., Muthukumar, M.: Rotational relaxation time as unifying time scale for polymer and fiber drag reduction. Phys. Rev. E **93**(5), 052503 (2016)
14. Xi, L., Bai, X.: Marginal turbulent state of viscoelastic fluids: a polymer drag reduction perspective. Phys. Rev. E **93**(4), 043118 (2016)
15. Oldroyd, J.G.: Proceedings 1st International Congress on Rheology, vol. 2. North-Holland (1949)
16. Tanner, R.I., Walters, K.: Rheology: An Historical Perspective. Elsevier, Amsterdam (1998)
17. De Gennes, P.-G.: Introduction to Polymer Dynamics. Cambridge University Press, Cambridge (1990)
18. L'vov, V.S., Pomyalov, A., Procaccia, I., Tiberkevich, V.: Drag reduction by polymers in wall bounded turbulence. Phys. Rev. Lett. **92**(24), 244503 (2004)
19. Procaccia, I., L'vov, V.S., Benzi, R.: Colloquium: theory of drag reduction by polymers in wall-bounded turbulence. Rev. Mod. Phys. **80**(1), 225 (2008)
20. Lumley, J.L.: Drag reduction by additives. Annu. Rev. Fluid Mech. **1**, 367–384 (1969)
21. Reynolds, O.: An experimental investigation of the circumstances which determine whether the motion of water shall be direct or sinuous, and of the law of resistance in parallel channels. Philos. Trans. R. Soc. Lond. **174**, 935–982 (1883)
22. Reynolds, O.: On the dynamical theory of incompressible viscous fluids and the determination of the criterion. Philos. Trans. R. Soc. Lond. **186**, 123–164 (1895)
23. Faisst, H., Eckhardt, B.: Sensitive dependence on initial conditions in transition to turbulence in pipe flow. J. Fluid Mech. **504**, 343–352 (2004)
24. Eckhardt, B.: Turbulence transition in pipe flow: some open questions. Nonlinearity **21**(1), T1 (2007)
25. Eckhardt, B.: Introduction. Turbulence transition in pipe flow: 125th anniversary of the publication of Reynolds' paper. Philos. Trans. R. Soc. A Math. Phys. Eng. Sci. **367**(1888), 449–455 (2009)
26. Avila, K., et al.: The onset of turbulence in pipe flow. Science **333**(6039), 192–196 (2011)
27. Romanov, V.A.: Stability of plane-parallel Couette flow. Funct. Anal. Appl. **7**(2), 137–146 (1973)
28. Landau, L.D., Lifshitz, E.M.: Fluid Mechanics. Elsevier, Amsterdam (2013)
29. Peixinho, J., Mullin, T.: Decay of turbulence in pipe flow. Phys. Rev. Lett. **96**(9), 094501 (2006)
30. Wygnanski, I.J., Champagne, F.: On transition in a pipe. Part 1. The origin of puffs and slugs and the flow in a turbulent slug. J. Fluid Mech. **59**(2), 281–335 (1973)
31. Volokh, K.: An investigation into the stability of a shear thinning fluid. Int. J. Eng. Sci. **47**(5–6), 740–743 (2009)
32. Volokh, K.: Navier–Stokes model with viscous strength. Comput. Model. Eng. Sci. **92**, 87–101 (2013)
33. Raghavan, B., Ostoja-Starzewski, M.: Shear-thinning of molecular fluids in Couette flow. Phys. Fluids **29**, 023103 (2017)
34. Lahiri, S.K., Volokh, K.Y.: Transition from laminar to turbulent pipe flow as a process of growing material instabilities. Submitted
35. ANSYS: ANSYS Fluent Theory Guide 15.0. ANSYS, Canonsburg (2013)
36. Smagorinsky, J.: General circulation experiments with the primitive equations: I. The basic experiment. Mon. Weather Rev. **91**(3), 99–164 (1963)
37. Nicoud, F., Ducros, F.: Subgrid-scale stress modelling based on the square of the velocity gradient tensor. Flow Turbul. Combust. **62**(3), 183–200 (1999)